sciendo
ISSN 1335-8871
MEASUREMENT SCIENCE REVIEW
Journal homepage: https://content.sciendo.com

Testing the Performance of the Video Camera to Monitor the Vertical Movements of the Structure via a Specially Designed Steel Beam Apparatus

Mehmet Eren*, Ramazan Gürsel Hoşbaş

Department of Geomatic Engineering, Yildiz Technical University, Davutpaşa, 34220, Istanbul, Turkey, meren@yildiz.edu.tr

Abstract: This article focuses on a specially designed steel beam testing apparatus to determine the dynamics of the structure using data obtained from different sensor systems. The analysis of these different sensor systems is performed by processing data recorded by the Global Navigation Satellite System (GNSS), vision based measurement (video camera), and accelerometer surveys. To perform this analysis, the accelerometer and GNSS receiver are installed at the steel beam's mid-span position. The high-contrast artificial target attached to the accelerometer is recorded by a video camera to monitor the structural dynamics. Steel beam experiments show that it is compatible with the accelerometer, which is predicted as a reference sensor in detecting motion with an amplitude of 10 mm and above in the vertical direction with GNSS and determining the structural frequency by spectral analysis. On the other hand, we concluded that the video camera can be used to determine the structural dynamics in SHM because its results were compatible with the reference data even if the amplitude was too small.

Keywords: SHM, vision-based measurement, vertical displacement, kinematic PPP, GNSS, frequency.

1. INTRODUCTION

Wind, traffic load, temperature, and water loads are examples of forces that can impact any structure. These forces induce deflection, elevation, and torsion, determining the movements, which are the ultimate focus of Structural Health Monitoring (SHM). SHM technology is needed due to the high cost of such engineering structures and, more importantly, public safety management. Structural health monitoring is a series of processes that have four steps: determining the appropriate detection system, collecting data, interpreting the information obtained, and determining the damage and taking the necessary precautions (evacuating the structure or repairing the damage). Many measuring instruments are used for SHM (extensometer, tiltmeter, micrometer, accelerometer [1], GNSS (Static, Kinematics, Real Time Kinematics (RTK), and Precision Point Positioning (PPP)) [2], robotic total station (RTS) [3], vision-based measurement [4], laser vibrometer [5]). To estimate the structure's performance under various loads and structural conditions, the relevant structure is simulated on a computer and displacements are monitored using the finite element method (FEM) [6], [7]. The displacement movements take the form of sine waves (the number of waves per unit time equals the frequency value provided for the structure's displacement). Since the acting loads and the size of the changes observed on the structure are the parameters for structural damage, calculating the frequency value is of particular importance. Therefore, it was investigated in [8] whether the natural frequencies and rigidity of the stiffening girder are preserved during a typhoon. A measurement device with appropriate sampling frequencies must be used to conduct measurements. The maximum frequency value that any measuring instrument can establish is half of the sampling frequency (Nyquist frequency).

Although GNSS was initially developed for military and navigation applications, it is now one of the essential SHM technologies. There are several studies on this topic in the literature, and the use of GNSS in SHM was accomplished for the first time with the work performed by [9]. The relative position changes were observed by establishing a GPS station on the top of the 160 m high Calgary Tower. It is supported by many GNSS-based SHM solution techniques, including Precise Positioning Kinematic (PPK), Real Time Kinematics (RTK), Network RTK (NRTK), and Precise Point Positioning (PPP) solutions. PPP GNSS is a technique in which the point position is accurately determined using precise satellite orbit, clock, and bias corrections anywhere in the world with the help of a single satellite receiver. Most research papers in the

DOI: 10.2478/msr-2023-0004

*Corresponding author: meren@yildiz.edu.tr (M. Eren)

literature use relative GNSS positioning solutions, and since 2010, numerous commercial PPP calculation tools have been implemented to support the results in monitoring SHM and communicating precise corrections in real time. According to [10], it was found that the kinematic PPP solution can detect horizontal vibrations with amplitudes of less than 1 cm and vertical vibrations with amplitudes of about 1-1.5 cm with high reliability. PPP can perform centimeter-level high-precision locations using accurate satellite orbit and clock data [11], [12].

In the conventional satellite-based approach, the displacements of a structure induced by dynamic processes are monitored using a GNSS receiver embedded in the structure. Assuming that the point coordinates of the structures are monitored by static GNSS measurements, the calculations are often based on the average of the structure observed in an interval of 30 second or more [13]. Because of the disadvantages of accelerometers [14] in measuring low-frequency structural displacements and GNSS in low-amplitude displacements, both accelerometers and GNSS [15], [16] should be integrated into SHM. As a result, GNSS and accelerometer measurements are often analyzed separately in the form of a post-process for the integration of displacement data collected by both methods.

Using innovative approaches, GNSS directly retrieves the coordinates of any monitored moving object, despite the constraints imposed by satellite geometry that can impact measurement accuracy. The significant contribution of such innovative methods enables the instantaneous coordinates of stations and sinusoidal waveforms to be determined by analyzing high frequency data (data rated at 1 Hz or more). The high rate GNSS method is widely used for SHM. It demonstrated the ability of a high-speed Global Positioning System (GPS) to detect and monitor the dynamic deformation of structures such as towers, tall buildings, bridges, and structural health [17], [18]. For example, the technical feasibility [15] of using GPS to monitor deformations in dynamic structures due to winds, traffic, earthquakes, and similar loading has been proven in the United Kingdom [19] and Japan [20]. During the 2009 earthquake that struck L'Aquila, Italy (Mw 6.3), a single 10 Hz receiver reconstructed for the first time the waveforms of the displacements at a frequency of 10 Hz [21]. The sample study was conducted at a frequency of 50 Hz. [22]. The structural analyses in [23] were performed using a GNSS receiver with a sampling rate of 100 Hz and accelerometers (100-200 Hz). Data loss is avoided if structural displacements are accurately perceived and data is collected at a high frequency [24].

In acquiring data with the help of image-based sensors (camera), there is no need for physical contact with the structure to be measured as in the traditional method. With lower cost and less labor than other methods, hundreds of meters away from the building, the information about the building is obtained with high accuracy from multiple points entering the image, not from a single point as in traditional methods [25]. In SHM applications, the displacement magnitude and natural structure frequencies can be determined using displacement data obtained from single or more camera measurements. In this process, the camera is mounted on a tripod away from the structure and directed to the target, and data collection begins. These obtained data are evaluated in real time if data processing software is available. Otherwise, these recorded data are considered as post-process. Since the camera is installed away from the structure to be monitored, a camera with the appropriate magnification should be used. The reason for this is that the pixel density (number of pixels per mm) must be high in order to detect the structure's motion with high accuracy. This accuracy depends on the camera type and the camera's distance from the target [26].

Displacement operation methods such as Feature Point Matching, Optical Flow Estimation, Template Matching, and Background Subtraction are used. They save time by limiting the natural (screw, beam, etc.) and artificial targets on the object to be measured to a predefined region of interest (ROI) instead of searching the entire video frame. Consideration should be given to the ROI being large enough to cover its potential position in the next frame. In this study, a Template Matching algorithm based on the principle of tracking a target across the entire video recording was used to determine displacements and frequencies. Template Matching is a very intensive computational procedure aimed to find a pattern within an image [25]. In obtaining vision-based data, structural dynamics are determined by using artificial or natural targets [27] on the structure. Busca et al. (2013) stated that artificial targets help one to obtain more precise results than the natural targets [28]. Therefore, we preferred to use the artificial targets.

Accelerometers, which measure the acceleration of a moving object, have a wide range of uses, including navigation and guiding systems, military applications, biomedical applications, and SHM. The mechanism of operation of accelerometers is based on Newton's second law of motion. Accelerometer sensors based on Micro Electromechanical Systems (MEMS) can monitor mechanical vibrations in engineering applications. Their use has increased significantly due to their low cost, power efficiency and small size [29].

On the Binzhou Yellow River Highway Bridge, an online service SHM consisting of accelerometers and a GPS receiver was installed to monitor acceleration and displacement in the time frequency and to show the observed responses of the bridge exposed to moving vehicle loads [30]. Moreover, to measure the natural frequencies of a pedestrian suspension bridge, a hybrid SHM system consisting of GNSS and a three-axis accelerometer was used in [24] to eliminate deficiencies of both measuring technologies. A Robotic Total Station (RTS), a GNSS receiver, and an accelerometer were installed, and tests on a horizontally freely oscillating oscillator were performed [31]. In addition, the vertical oscillation detection capability of the kinematic PPP solution of engineering structures was tested using the GNSS receiver installed on a steel bar to simulate a flexible structure [32].

Spectral analysis is used to analyze signal frequency characteristics. For this purpose, the Fast Fourier Transform (FFT) is used. With FFT analysis, procedures such as calculating the amplitude and frequency values of the signals are carried out effectively [33].

The acceleration data from the accelerometers and the displacement parameters generated from these data can also be used to monitor structural health. The relative displacement movements calculated by the accelerometer are in mm accuracy depending on the sensor's resolution, while GNSS is in the cm range. On the other hand, the accuracy of the vision-based system varies between 0.5-0.01 pixels [34].

In this study, the steel beam in equilibrium was pushed by hand from the mid-point, and a free oscillating motion was generated. It is aimed to monitor a structure's dynamic displacement response and calculate its natural frequency within the framework of structural health monitoring procedures in engineering structures using three separate measuring devices. For this purpose, high-rate GNSS measurements, vision-based data, and MEMS accelerometer measurements were performed. The high-contrast artificial target attached to the accelerometer is recorded by a video camera to monitor the structural dynamics.

2. METHODS

A. Data

This study collected data with three different measuring instruments placed on a specially designed steel beam test setup (Fig. 1). A data collection mechanism for the steel beam test was performed by placing a 7.00 m long steel beam on a football field (Fig. 2). The BWT901CL accelerometer and Topcon Hiper SR GNSS receiver were installed at the steel beam's mid-span position. Data were collected from the target placed on MEMS with a Nikon P900 video camera at 65, 145, and 200 m distances, respectively.

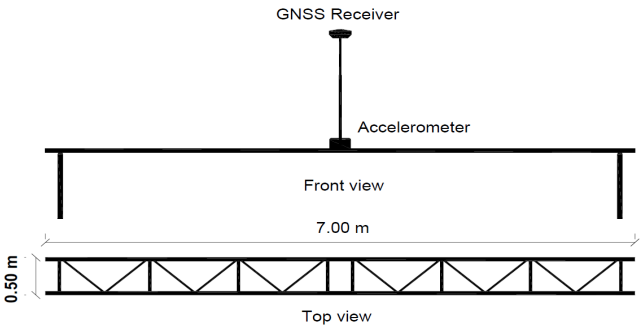

Fig. 1. Scheme of the steel beam measuring device.

MEMS and video camera data were obtained at 50 Hz data frequency, while static measurements were taken at 10 Hz data frequency. A vertical motion with random amplitude was applied externally to the steel beam, and the simple harmonic motion in the vertical direction was maintained. Data were obtained concurrently from all devices, and the accelerometer data were used as the reference data. The technical information of the measuring devices used in the experiment is given in Table 1.

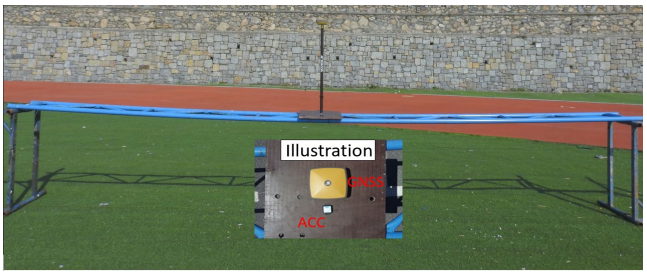

Fig. 2. A view of the steel beam measuring setup.

Table 1. Technical information of measuring instruments used in data collection.

Data collection method	Measurement sensitivity / resolution
Topcon Hiper SR	H:3 mm+1.0 ppm V:5 mm+1.0ppm
WIT BWT901CL	0.005 g
Nikon P900	1920x1080, 60 fps, 83X optical zoom

SHM systems can produce automated structural health assessments by processing data from sensors on the structure. Wired systems are often employed in SHM, but they have disadvantages such as time-consuming wiring, high cost, additional labor, etc. Therefore, wireless sensor was preferred in this study (Fig. 3).

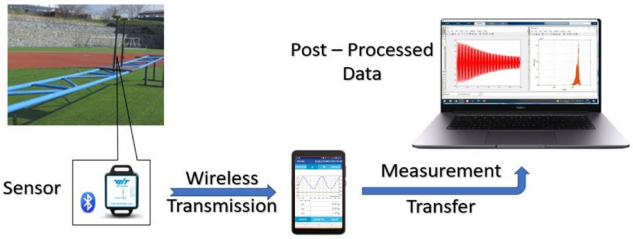

Fig. 3. Wireless accelerometer system configuration.

B. Data analysis

With the help of these coordinate data, the standard deviation values were calculated and interpreted statistically. After these processes, shaking table and steel beam tests were carried out.

The least squares method is widely used in determining harmonic motions and removing outliers [35], [36].

When the time series of the measurement values in Fig. 4 and Fig. 5 are examined, residuals and ±3σ values are seen. From horizontal components; East: max.: 5.5 mm, min.: -5.4 mm and standard deviation:1.5 mm, North max.: 7.8, min.: -7.5 and standard deviation value was calculated as 2.3 mm. On the other hand, the vertical component is weaker than the horizontal component [37] and has 2-3 times lower measurement accuracy than the horizontal [38]. It was used similarly in this study (Fig. 9).

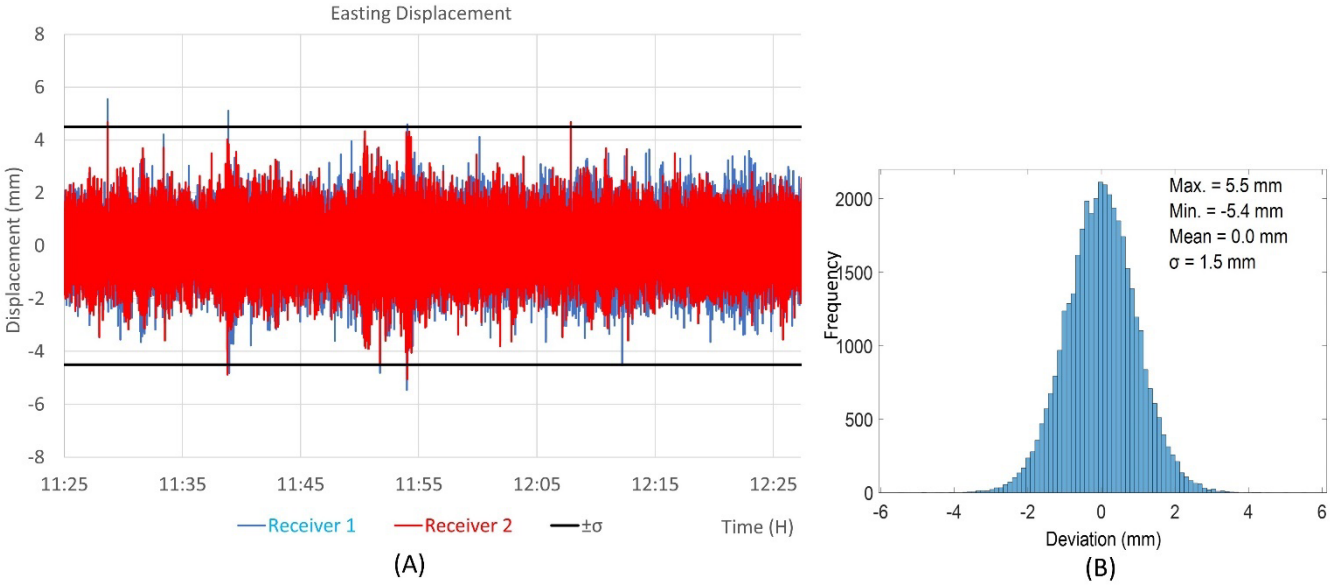

Fig. 4. Residuals and ±3σ for GNSS measurement East component (A) and the Histogram of Residuals (B).

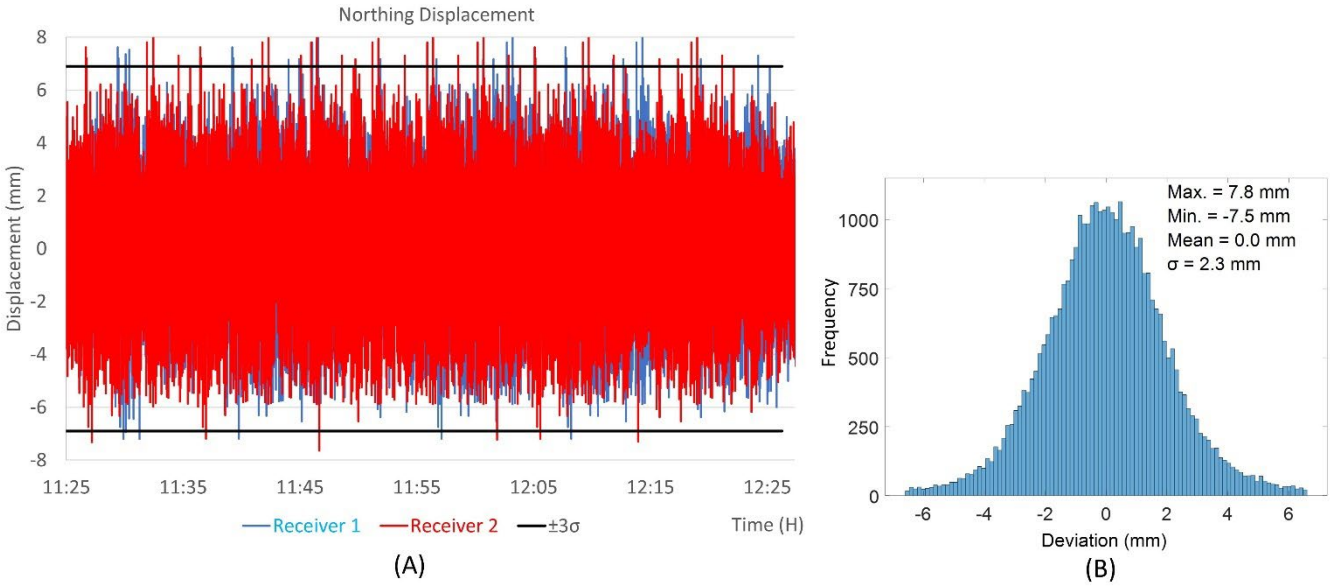

Fig. 5. Residuals and ±3σ for GNSS measurement North component (A) and the Histogram of Residuals (B).

C. Shaking table calibration measurement

The BWT901CL accelerometer, which produces 200 Hz data and can transmit via Bluetooth, and the video camera used in the study were subjected to calibration measurements to test their usability. In this context, an accelerometer was placed on the shaking table, a video camera was installed 10 m away from the shaking table, and measurements were made. In contrast, the shaking table was set to 100 mm amplitude and 0.1 Hz frequency range on the computer, LVDT 1000 Hz, BWT901 CL 100 Hz, and camera 50 Hz data recording frequency, respectively. The data received by these two sensors are compared with the reference data LVDT - which is placed on the shaking table pistons at the production stage. While the video camera data was converted into displacement data with the help of image processing codes in Matlab 2018b software, LVDT data was directly received by the computer as displacement data.

On the other hand, the accelerometer data were analyzed in Matlab 2018b software, and the displacement data were obtained from the accelerator data. The measured acceleration data were subjected to a series of processing. These transactions are:

- The acceleration data set, whose initial and last values end with zero, was taken.
- The received data set, frequencies outside the range of 4.5 to 0.2 Hz (cutoff frequency) were filtered with high pass and low pass filter (6th-degree polynomial using butter windowing).

- Displacement data was obtained using numerical integration twice with the Midpoint Rule filtered data.
- The data has been extracted with the Baseline Correction process originating from the integration constants.

Data from three different sensors were collected and compared in a time series (Fig. 6). These results showed that the data obtained from the BWT901CL accelerometer with a recording capacity of 100 Hz and a video camera with a recording capacity of 50 fps are comparable to the data obtained from the 1000 Hz LVDT.

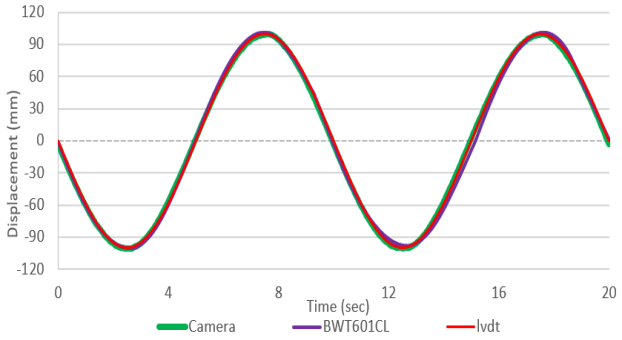

Fig. 6. The displacement graph was obtained by evaluating the data collected by all three methods.

Pearson correlation coefficients, which measure the linear relationship between two variables, were statistically calculated between the LVDT data, MEMS, and the camera data. The correlation coefficient (r) between the measures is greater than 95% for all data (Table 2). Moreover, when Fig. 6 is examined, it is seen that the camera data are more compatible with the LVDT than the accelerometer data. The obtained displacement data reveal that both systems are consistent with the reference data and can be used in future studies.

Table 2. Statistical calculations on measurements.

Data collection method	Correlation coefficient (r)	RMS (mm)
LVDT	Reference sensor	70.64
BWT901CL	0.992	70.26
Camera	0.997	70.24

D. Steel beam experiment

The vertical displacement was determined using an accelerometer, video camera, and GNSS data, and the discrepancies among the results produced by different methods were compared. Initially, the applicability of the WIT BWT901CL brand accelerometer on the experimental shaking table was established to determine the use of methods to be employed in assessing deformation/ displacement, and then combined measurement data were used in the applications and performed on the steel beam.

GNSS measurements were used in the static mode and then were processed using CSRS PPP and Topcon Magnet Tools version 7.2.0 software for kinematic solution. To ensure compatibility among the data of the three methods, the height values collected by GNSS were converted into displacement data. Relative displacement values were obtained by subtracting that dataset's average height value from each height data obtained by the kinematic PPP.

The acceleration data obtained using the BWT901CL accelerometer were analyzed using the codes developed in the Matlab 2018 b v. program, and the displacement values were generated.

Camera data within the scope of the study, the Template Matching method was evaluated with the help of a smart search technique developed by [39]. The data obtained with the video camera were subjected to image processing in the Matlab 2018 b v. software (Fig. 7).

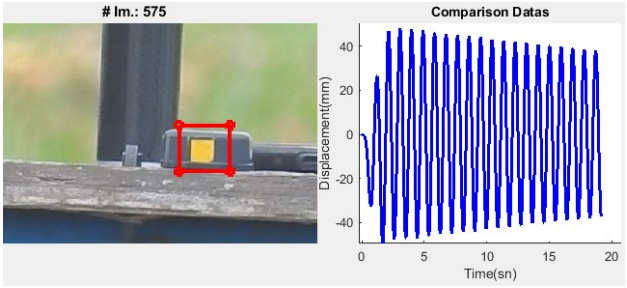

Fig. 7. A view of the image processing done in the Matlab software.

The displacement values obtained from each of the three methods were subjected to FFT analysis in the Matlab 2018 b software, and it was examined whether the obtained variations in frequency values were statistically significant.

3. RESULTS AND DISCUSSION

The spectral analysis of the vertical displacement among all three methods was performed in the Matlab 2018 b software, and the Eigen(natural) frequency values of each method were computed from the FFT analysis results, as shown in Table 3.

Table 3. Frequency values using FFT analysis.

Data collection method	Frequency (Hz)	Error (%)
BWT901CL	2.112	Reference
Nikon P900	2.114	0.094
Kinematics PPP	2.115	0.142

Fig. 9. Data for three measuring systems were incorporated into local time.

The frequency values received from the BWT901CL accelerometer, and the kinematic PPP solution were found to be quite close when the frequency values were compared.

The smoothness of the waveform predominates the natural frequency value derived from the FFT analysis in places where the amplitude values received from GNSS data are 10 mm or more (between 11:50:39 and 11:51:32 hours). Fig. 10(A) (Frequency-Power Spectral Density (PSD)) and Fig. 10(A) show the ability to detect vertical motion.

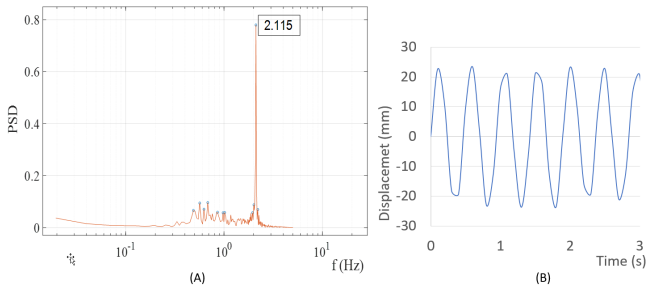

Fig. 10. Frequency graph (A) and motion waveform (B) of the zone.

In addition, when the displacement data obtained from all measuring instruments in the field when the size is greater than 10 mm are examined closely, it is seen that they are very compatible with each other despite the differences (Fig. 11).

Fig. 11. Graph of displacement values in the region where the amplitude value is greater than 10 mm.

When the amplitude value is less than 10 mm, both distortions in the sinusoidal forms and a lack of dominant frequency are observed. However, a frequency value was obtained when the FFT analysis was performed (Fig. 12). The reason for these distortions is assumed to be the GNSS surveys.

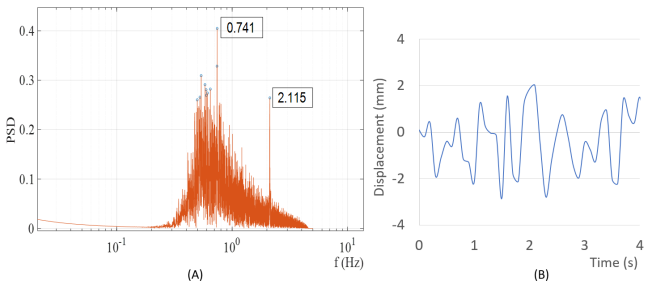

Fig. 12. Frequency graph (A) and motion waveform (B).

When the displacement/deformation amplitude value was analyzed, it was found that the time with the lowest value in the series was about 12:39 h. When the 4-second data within this time period is reviewed, it is noted that the accelerometer data has an amplitude of 2 mm, and there is no deformation in the waveform, implying that it can determine displacement values of at least 4 mm (Fig. 13).

Even though the displacement values obtained with the kinematic PPP solution appear in the same graph at about 3-5 mm, the waveform was distorted and inappropriate for measuring the frequency values. If the values from GNSS displacement amplitudes are less than 10 mm, the displacement value computed by the receiver appears as a random value.

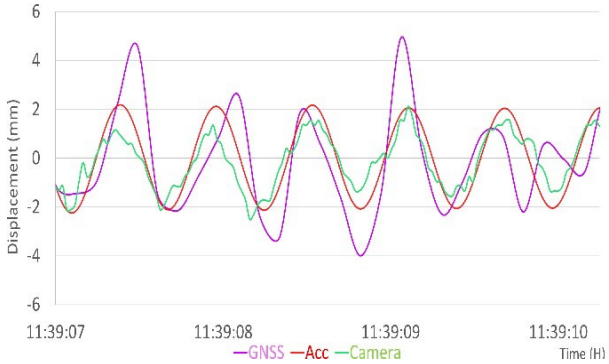

Fig. 13. Graph of displacement values in the region where the amplitude value is less than 10 mm.

It was observed that the displacement data obtained with the video camera yielded better results than those obtained from the GNSS measurements. However, since vision-based measures are related to light, the camera causes fluctuations in the wave crests due to the refraction of the data. Even in this state, it does not have a problem determining the frequency. Points to be considered to minimize the errors in the displacement: heat, measuring distance, the height difference of the measuring camera and the target from the ground, water vapor in the environment, etc., are factors that affect the measurement results.

By taking the aforementioned effects into account, displacement can be determined with a few mm sensitivity.

4. CONCLUSIONS

Concurrent data collected by three separate measurement tools were examined in this study, and vertical displacement values were computed by using the data.

The vibration that emerges from a force applied to the structure or induced by the measured object's structure is a parameter of the damage that will develop in the structure.

While collecting video camera data, errors occur in the displacement values due to light refraction. The time interval where these effects are the least (temperature, camera, and target height, measurement distance, etc.) should be selected. When these effects are minimized, results will be noticeably improved and data with mm accuracy will be obtained.

There are discrepancies in the amplitudes received from the GNSS data and the accelerometer data in the steel beam test. While determining the displacement with GNSS measurements, the amplitude of the movement of the structure is less than 10 mm - especially in the vertical direction - it cannot give reliable results.

It is found that even with the camera data taken from a distance of 200 m, very compatible data are obtained, where the sinusoidal form is not distorted. It can determine the dynamics of the structure with the measurements to be made alone.

REFERENCES

[1] Morichika, S., Sekiya, H., Zhu, Y., Hirano, S., Maruyama, O. (2021). Estimation of displacement response in steel plate girder bridge using a single MEMS accelerometer. *IEEE Sensors Journal*, 21 (6), 8204-8208. https://doi.org/10.1109/JSEN.2021.3051697

[2] Koch, I.E., Veronez, M.R., da Silva, R.M., Klein, I., Matsuoka, M.T., Gonzaga, L., Larocca, A.P.C. (2017). Least trimmed squares estimator with redundancy constraint for outlier detection in GNSS networks. *Expert Systems with Applications*, 88, 230-237. https://doi.org/10.1016/j.eswa.2017.07.009

[3] Dos Santos, R.C., Larocca, A.P.C., de Araújo Neto, J.O., Barbosa, A.C.B., Oliveira, J.V.M. (2019). Detection of a curved bridge deck vibration using robotic total stations for structural health monitoring. *Journal of Civil Structural Health Monitoring*, 9, 63-76. https://doi.org/10.1007/s13349-019-00322-1

[4] Dong, C.-Z., Celik, O., Catbas, F.N., O'Brien, E.J., Taylor, S. (2020). Structural displacement monitoring using deep learning-based full field optical flow methods. *Structure and Infrastructure Engineering*, 16 (1). https://doi.org/10.1080/15732479.2019.1650078

[5] Beben, D. (2016). Application of interferometry method for dynamic continuous testing of bridges. *Periodica Polytechnica Civil Engineering*, 60 (3), 387-395. https://doi.org/10.3311/PPci.8679

[6] Fei, Q.G., Xu, Y.L., NG, C.L., Wong, K.Y., Chan, W.Y., Man, K.L. (2007). Structural health monitoring oriented finite element model of Tsing Ma bridge tower. *International Journal of Structural Stability and Dynamics*, 07 (04), 647-668. https://doi.org/10.1142/S0219455407002502

[7] Wang, X., Zhao, Q., Xi, R., Li, C., Li, G., Li, L. (2021). Review of bridge structural health monitoring based on GNSS: From displacement monitoring to dynamic characteristic identification. *IEEE Access*, 9, 80043-80065. https://doi.org/10.1109/ACCESS.2021.3083749

[8] Ju, M., Park, C., Kim, G. (2015). Structural Health Monitoring (SHM) for a cable stayed bridge under typhoon. *KSCE Journal of Civil Engineering*, 19 (4), 1058-1068. https://doi.org/10.1007/s12205-015-0039-3

[9] Lovse, J.W., Teskey, W.F., Lachapelle, G., Cannon, M.E. (1995). Dynamic deformation monitoring of tall structure using GPS technology. *Journal of Surveying Engineering*, 121 (1), 35-40. DOI: 10.1061/(ASCE)0733-9453(1995)121:1(35).

[10] Bisnath, S., Gao, Y. (2009). Precise point positioning. *GPS World*, 20, 43-50.

[11] Xu, P., Shi, C., Fang, R., Liu, J., Niu, X., Zhang, Q., Yanagidani, T. (2013). High-rate precise point positioning (PPP) to measure seismic wave motions: An experimental comparison of GPS PPP with inertial measurement units. *Journal of Geodesy* 87 (4), 361–372. https://doi.org/10.1007/s00190-012-0606-z

[12] Zumberge, J.F., Heflin, M.B., Jefferson, D.C., Watkins, M.M., Webb, F.H. (1997). Precise point positioning for the efficient and robust analysis of GPS data from large networks. *Journal of Geophysical Research: Solid Earth*, 102 (B3), 5005-5017. https://doi.org/10.1029/96JB03860

[13] Erkoç, M.H., Doğan, U., Yıldız, H., Sezen, E. (2022). Estimation of vertical land motion along the south and west coast of Turkey from multi-sensor observations. *Advances in Space Research*, 70 (7), 1761-1772. https://doi.org/10.1016/j.asr.2022.06.022

[14] Moschas, F., Avallone, A., Saltogianni, V., Stiros, S.C. (2014). Strong motion displacement waveforms using 10-Hz precise point positioning GPS: An assessment based on free oscillation experiments. *Earthquake Engineering & Structural Dynamics*, 43 (12), 1853-1866. https://doi.org/10.1002/eqe.2426

[15] Wieser, A., Brunner, F. (2002). Analysis of bridge deformations using continuous GPS measurements. In *2nd Conference of Engineering Surveying (INGEO 2002)*. Bratislava, Slovakia: Slovak University of Technology, 45-52.

[16] Çelebi, M. (2000). GPS in dynamic monitoring of long-period structures. *Soil Dynamics and Earthquake Engineering*, 20 (5-8), 477-483. https://doi.org/10.1016/S0267-7261(00)00094-4

[17] Watson, C., Watson, T., Coleman, R. (2007). Structural monitoring of cable-stayed bridge: Analysis of GPS versus modeled deflections. *Journal of Surveying Engineering*, 133 (1), 23-28. DOI: 10.1061/(ASCE)0733-9453(2007)133:1(23).

[18] Schaal, R.E., Larocca, A.P. (2009). Measuring dynamic oscillations of a small span cable-stayed footbridge: Case study using L1 GPS receivers. *Journal of Surveying Engineering*, 135 (1), 33-37. DOI: 10.1061/(ASCE)0733-9453(2009)135:1(33).

[19] Ashkenazi, V., Roberts, G.W. (1997). Experimental monitoring of the Humber Bridge using GPS. *Proceedings of the Institution of Civil Engineers - Civil Engineering*, 120 (4), 177-182. https://doi.org/10.1680/icien.1997.29810

[20] Tamura, Y., Matsui, M., Pagnini, L.-C., Ishibashi, R., Yoshida, A. (2002). Measurement of wind-induced response of buildings using RTK-GPS. *Journal of Wind Engineering and Industrial Aerodynamics*, 90 (12-15), 1783-1793. https://doi.org/10.1016/S0167-6105(02)00287-8

[21] Avallone, A., Marzario, M., Cirella, A., Piatanesi, A., Rovelli, A., Di Alessandro, C., Mattone, M. (2011). Very high rate (10 Hz) GPS seismology for moderate-magnitude earthquakes: The case of the Mw 6.3 L'Aquila (central Italy) event. *Journal of Geophysical Research: Solid Earth*, 116 (B2). https://doi.org/10.1029/2010JB007834

[22] Genrich, J.F., Bock, Y. (2006). Instantaneous geodetic positioning with 10-50 Hz GPS measurements: Noise characteristics and implications for monitoring networks. *Journal of Geophysical Research: Solid Earth*, 111 (B3). https://doi.org/10.1029/2005JB003617

[23] Psimoulis, P.A., Stiros, S.C. (2012). A supervised learning computer-based algorithm to derive the amplitude of oscillations of structures using noisy GPS and Robotic Theodolites (RTS) records. *Computers & Structures*, 92-93, 337-348. https://doi.org/10.1016/j.compstruc.2011.10.019

[24] Moschas, F., Stiros, S. (2015) Dynamic deflections of a stiff footbridge using 100-Hz GNSS and accelerometer data. *Journal of Surveying Engineering*, 141 (4). DOI: 10.1061/(ASCE)SU.1943-5428.0000146.

[25] Feng, D., Feng, M.Q. (2018). Computer vision for SHM of civil infrastructure: From dynamic response measurement to damage detection – A review. *Engineering Structures*, 156, 105-117. https://doi.org/10.1016/j.engstruct.2017.11.018

[26] Busca, G., Cigada, A., Mazzoleni, P., Zappa, E. (2013). Vibration monitoring of multiple bridge points by means of a unique vision-based measuring system. *Experimental Mechanics*, 54 (2), 255-271. https://doi.org/10.1007/s11340-013-9784-8

[27] Feng, M.Q., Fukuda, Y., Feng, D., Mizuta, M. (2015). Nontarget vision sensor for remote measurement of bridge dynamic response. *Journal of Bridge Engineering*, 20 (12), 04015023. DOI: 10.1061/(ASCE)BE.1943-5592.0000747.

[28] Farrar, C.R., Darling, T.W., Migliori, A., Baker, W.E. (1999). Microwave interferometers for non-contact vibration measurements on large structures. *Mechanical Systems and Signal Processing*, 13 (2), 241-253. https://doi.org/10.1006/mssp.1998.1216

[29] Huang, M., Hou, C., Li, Y., Liu, H., Wang, F., Chen, T., Yang, Z., Tang, G., Sun, L. (2019). A low-frequency MEMS piezoelectric energy harvesting system based on frequency up-conversion mechanism. *Micromachines*, 10 (10), 639. https://doi.org/10.3390/mi10100639

[30] Li, H., Ou, J., Zhao, X., Zhou, W., Li, H., Zhou, Z., Yang, Y. (2006). Structural health monitoring system for the Shandong Binzhou Yellow River highway bridge. *Computer-Aided Civil and Infrastructure Engineering*, 21 (4), 306-317. https://doi.org/10.1111/j.1467-8667.2006.00437.x

[31] Erdoğan, H. (2006). *Mühendislik Yapılarındaki Dinamik Davranısların Jeodezik Ölçmelerle Belirlenmesi*. Doctoral dissertation, Yıldız Technical University, Institute of Science and Engineering, Istanbul, Turkey. (in Turkish)

[32] Yigit, C.O. (2016). Experimental assessment of post-processed kinematic Precise Point Positioning method for structural health monitoring, *Geomatics*, *Natural Hazards and Risk*, 7 (1), 360-383. https://doi.org/10.1080/19475705.2014.917724

[33] Yigit, C.O., Gurlek, E. (2017). Experimental testing of high-rate GNSS precise point positioning (PPP) method for detecting dynamic vertical displacement response of engineering structures, *Geomatics, Natural Hazards and Risk*, 8 (2), 893-904. https://doi.org/10.1080/19475705.2017.1284160

[34] Pan, B., Xie, H., Xu, B., Dai, F. (2006). Performance of sub-pixel registration algorithms in digital image correlation. *Measurement Science and Technology*, 17 (6), 1615-1621. https://doi.org/10.1088/0957-0233/17/6/045

[35] Erkoç, M.H., Doğan, U. (2022). Regional tidal modelling using tide gauges and satellite altimetry data in south-west coast of Turkey. *KSCE Journal of Civil Engineering*, 26, 4052-4061. https://doi.org/10.1007/s12205-022-0320-1

[36] Kim, K.B., Lee, S.B. (2002). Determination of gravity anomaly using satellite altimeter data in the Great Lakes. *KSCE Journal of Civil Engineering*, 6 (3), 313-320. https://doi.org/10.1007/BF02829153

[37] Ata, E., Pirti, A., Hoşbaş, R.G. (2018). Testing height accuracy in CORS-TR technique. In *FIG Congress 2018*. Istanbul, Turkey.

[38] Wdowinski, S., Bock, Y., Zhang, J., Fang, P., Genrich, J. (1997). Southern California permanent GPS geodetic array: Spatial filtering of daily positions for estimating coseismic and postseismic displacements induced by the 1992 Landers earthquake. *Journal of Geophysical Research: Solid Earth,* 102 (B8), 18057-18070. https://doi.org/10.1029/97JB01378

[39] Avcı N., Alemdar, F. (2019). Sarsma masası testlerindeki dinamik parametrelerin görüntü işleme yöntemi ile ölçülmesi. *DÜMF Mühendislik Dergisi*, 10 (3), 1099-1112. https://doi.org/10.24012/dumf.524027 (in Turkish)

Received June 02, 2022
Accepted January 03, 2023